Earth and Planetary Science Letters 371–372 (2013) 16–25

Contents lists available at SciVerse ScienceDirect

Earth and Planetary Science Letters

journal homepage: www.elsevier.com/locate/epsl

# Seasonal changes in ice sheet motion due to melt water lubrication

I.J. Hewitt [1]

*Department of Mathematics, University of British Columbia, #121, 1984 Mathematics Road, Vancouver, BC, Canada V6T 1Z2*

ARTICLE INFO

*Article history:*
Received 24 January 2013
Received in revised form
10 April 2013
Accepted 12 April 2013
Editor: P. Shearer

*Keywords:*
ice sheet
hydrology
glacier
modelling

ABSTRACT

A numerical model is used to calculate how the motion of an idealized ice-sheet margin is affected by the subglacial drainage of melt water from its surface. The model describes the evolution of the drainage system and its coupling with ice flow through a sliding law that depends on the effective pressure. The results predict ice acceleration during early summer when the inefficient drainage system is temporarily overwhelmed. The growth of a more efficient drainage system leads to a subsequent slowdown of the ice very close to the margin, but high water pressure and ice velocity are maintained through much of the summer further inland. Annual mean ice velocity increases with the total quantity of melt water except close to the margin, where it is almost insensitive to the amount of melting. Short-term variability of melt water input leads to rapid changes in ice velocity that result in a slight increase in the mean velocity relative to a smoother input. Linked-cavity and poroelastic models for the distributed drainage system are compared, and their relative merits discussed. Two different sliding laws are considered, and the need for a holistic description of hydraulically controlled sliding is highlighted.



## 1. Introduction

Much interest has been generated recently in changes of ice motion at the margins of the Greenland ice sheet and the implications these have for its current and future mass balance. Significant variability in ice flow has been observed on time scales of hours to years (Rignot and Kanagaratnam, 2006; van de Wal et al., 2008; Das et al., 2008). Whilst it is not known how new such variability is, the implication is that the ice sheet can react rapidly to oceanic and climatic conditions.

In the case of ocean-terminating outlet glaciers, changes in ice speed are often attributed to changing conditions at the calving front (e.g. Joughin et al., 2008). In other areas, the speed of the ice is clearly influenced by lubrication at its base due to summer melt water descending from the surface (Shepherd et al., 2009; Hoffman et al., 2011). The purpose of this paper is to explore a model of the latter effect, providing a reference with which to interpret the current observations.

Following the established paradigm of alpine glaciers, the structure of the drainage system beneath the ice sheet margins is believed to evolve continually through the seasons (Bartholomew et al., 2010; Sole et al., 2011; Sundal et al., 2011). During winter, with no input from the surface, drainage pathways are squeezed closed and there is a poorly connected system with low transmissivity. When surface melt water reaches the bed in summer, this gives rise to high water pressures that have the effect of reducing basal resistance and increasing ice flow velocities. On the other hand, an increase in the capacity of the drainage system, aided by the melting of well-connected channels, may subsequently reduce water pressures and allow for slower ice velocities even with a larger quantity of melt water. At least, this is the general interpretation. In any case, it is uncertain how much farther (or less) a given section of ice will move in a year with, say, 50% more surface melting.

Numerical models provide a way to address that question, but most ice sheet models have included the effect of basal hydrology in only a rudimentary fashion, if at all. Those that have done so generally incorporate a water layer with a thickness that is directly related to water pressure. The basal shear stress resisting ice flow is then controlled by either the water pressure or the thickness of the water layer (e.g. Alley, 1996). The main application has been to study the evolution of ice streams, where basal melting or freeze-on control the thickness of the water layer. Transport of water is either ignored (Bougamont et al., 2011) or is accounted for by diffusion (Bueler and Brown, 2008; Sayag and Tziperman, 2008; van Pelt and Oerlemans, 2012), or by sheet flow driven by gradients of the ice pressure and basal topography (Johnson and Fastook, 2002; Le Brocq et al., 2009).

More sophisticated models have been proposed to describe the drainage system when a larger quantity of melt water is sourced from the ice surface (Flowers and Clarke, 2002; Creyts and Schoof, 2009; Schoof, 2010). Building on earlier concepts developed for alpine glaciers these models account for the evolving

*E-mail address:* hewitt@maths.ox.ac.uk
[1] Current address: Mathematical Institute, University of Oxford, 24-29 St Giles', Oxford, OX1 3LB.

0012-821X/$ - see front matter © 2013 Elsevier B.V. All rights reserved.
http://dx.doi.org/10.1016/j.epsl.2013.04.022

transmissivity of the drainage system. The only studies to combine them with ice dynamics are by Pimentel et al. (2010) and Pimentel and Flowers (2011), who demonstrate seasonal evolution of the drainage system and ice velocity in a flow-band model.

In this paper I combine two-dimensional plan-form models of the subglacial drainage system and ice dynamics. I apply the models to an idealized ice sheet margin with the goal to assess, for a simple generic case, what effect summer surface melting has on the speed of the ice. It would be a mistake to base quantitative predictions on these results given the continued uncertainty in some of the parameters; the intention is rather to explore the patterns of change that result.

The model necessarily contains a certain degree of complexity, but to interpret the results it is helpful to understand what is and is not included. The next section therefore explains the model as succinctly as possible, with more technical details included in the Supplementary material. Results of the calculations are shown in Section 3, and in Section 4 I discuss how robust these calculations are and how they compare to observations.

## 2. Model

### 2.1. Setup

The ice sheet considered in this paper is shown in Fig. 1. Its size, and the physical parameters used, are intended to be roughly appropriate for the Greenland margins. Even when the ice is moving quickly, the shape of the ice sheet on this scale will change only a small amount over the course of a year. The geometry is therefore treated as fixed. Ultimately, of course, one is interested in the longer term problem of how the ice sheet's motion alters its shape and size.

The model comprises two distinct components—a model for ice flow and a model for subglacial water flow, the base of the ice being assumed to be everywhere at the melting point. Coupling occurs through the basal friction law, which depends upon the subglacial water pressure, and through two feedbacks of the ice flow on the drainage system; namely, the opening of water-filled cavities and the melting caused by the frictional heating of the ice (the latter, as it turns out, is relatively unimportant for this study).

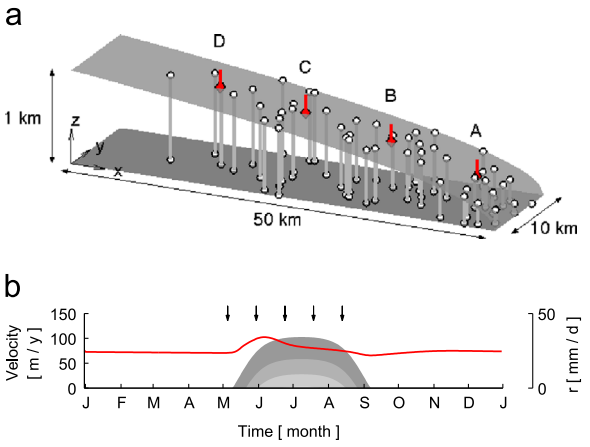


**Fig. 1.** (a) The ice sheet margin considered in this paper. Dots indicate the position of moulins that route water vertically to the bed; average moulin density is prescribed to increase with proximity to the margin. The bed is flat, $z=b=0$, and the surface is at $z=s=H_0\sqrt{1-x/x_0}$, where $H_0=1060$ m and $x_0=50$ km. (b) Example calculation of ice surface velocity at the position labelled A (red) in response to the idealized seasonal input $r$ (shaded; darkest shading is input at A, lighter shadings show corresponding input at B and C). The input decreases with elevation at lapse rate $r_s=60$ mm d$^{-1}$ km$^{-1}$, and is given by $r(s,t)=\max\{0,(r_m+r_s s_m)[\frac{1}{2}\tanh(t-t_{spr})/\Delta t-\frac{1}{2}\tanh(t-t_{aut})/\Delta t]-r_s s\}$, where $t_{spr}=135$ d, $t_{aut}=244$ d, $\Delta t=21$ d and $s_m=500$ m. The summer peak, and hence the spatial extent of melting, is controlled by the single parameter $r_m$, which corresponds to the peak rate at 500 m elevation. (For interpretation of the references to colour in this figure caption, the reader is referred to the web version of this article.)

The model is forced by a prescribed rate of water input from the ice surface, $r$, which varies according to an idealized seasonal cycle as shown in Fig. 1b. This represents all surface melt water and precipitation that is routed to the glacier bed (it may be distinct from the surface melt rate since no account is made of the supra- and en-glacial processes that convert the melting signal to the subglacial input; notwithstanding that, I often refer to $r$ as the melting rate). This inflow is routed to the subglacial drainage system through 50 moulins, the positions of which are randomly prescribed. The input to each moulin is taken from a surrounding catchment basin, $A_m$, based on a tessellation of the surface, i.e. the input is $R=\int_{A_m} r(s(x,y),t)\,\mathrm{d}x\,\mathrm{d}y$.

### 2.2. Ice flow

The model for ice flow is a vertically integrated approximation to the Stokes equations. It can be viewed as a combination of the 'shallow ice approximation' and 'membrane stress approximation', and is outlined in the Supplementary material (see also Schoof and Hindmarsh, 2010). It includes longitudinal and transverse stresses that are generated by variable slip at the bed and is therefore most suited to cases of relatively rapid sliding. Importantly, the driving stress due to the ice surface slope can be balanced by these additional stresses as well as by the basal shear stress.

Given the fixed ice geometry, described by basal elevation $z=b(x,y)$ and surface elevation $z=s(x,y)$, the model computes the horizontal velocity components $u(x,y,z)$ and $v(x,y,z)$ resulting from a basal friction law of the form

$$\boldsymbol{\tau}_b=f(U_b,N_+)\frac{\mathbf{u}_b}{U_b}, \tag{1}$$

where $\boldsymbol{\tau}_b$ is the basal shear stress, $\mathbf{u}_b=(u_b,v_b)\equiv(u(x,y,b),v(x,y,b))$ is the sliding velocity, and $U_b\equiv|\mathbf{u}_b|$ is the sliding speed. The function $f$ includes a dependence on the effective pressure, $N=p_i-p_w$, defined as the difference between the average ice normal stress, $p_i$, and the water pressure in the subglacial drainage system, $p_w$. In this ice flow approximation the ice normal stress is always hydrostatic, $p_i=\rho_i g H$, where $H(x,y)$ is the ice thickness, $\rho_i$ is the ice density, and $g$ is the gravitational acceleration. Negative effective pressures are treated as zero, so the sliding law more specifically depends on $N_+\equiv\max(N,0)$.

The function $f$ is a pivotal ingredient—it provides the means by which the hydraulic system influences ice motion. For this study I work with the assumption that this coupling occurs through $N$ alone. Specifically, some of the calculations employ a power law of the form

$$f(U_b,N)=\mu_a N^p U_b^q, \tag{2a}$$

where $\mu_a$ is a constant parameter and $p$ and $q$ are positive exponents, whilst some use a second law of the form

$$f(U_b,N)=\mu_b N\left(\frac{U_b}{U_b+\lambda_b A N^n}\right)^{1/n}, \tag{2b}$$

where $A$ and $n$ are the coefficients in Glen's law (see Supplementary material), $\lambda_b$ is a bed roughness length, and $\mu_b$ is a limiting roughness slope.

The form in (2a) has some empirical validation (Budd et al., 1979; Bindschadler, 1983), and has been used in a number of numerical ice sheet models (with different exponents; Fowler and Johnson, 1996; Alley, 1996; Bueler and Brown, 2008; van Pelt and Oerlemans, 2012; Bougamont et al., 2011). The form in (2b) is an attempt to capture the effect of cavitation (Fowler, 1986; Schoof, 2005), with a shift from the non-linear viscous drag

$f \approx \mu_b (\lambda_b A)^{-1/n} U_b^{1/n}$ when $N$ is large to the Coulomb-like behaviour $f \approx \mu_b N$ when $N$ is small. This is intended for hard bedrock, but may be appropriate for soft beds too, and was used in the models of Pimentel et al. (2010) and Pimentel and Flowers (2011).

### 2.3. Subglacial water flow

Subglacial drainage is thought to occur by a combination of distributed flow through sediments, thin films and linked cavities, and localized flow through channels that are melted upwards into the base of the ice (Fountain and Walder, 1998). A continuum model is difficult to construct, due to the eponymous tendency of the channels to channelize (Walder, 1982; Hewitt, 2011). The model is therefore based on a continuum 'sheet', described by an average thickness $h(x,y)$ and discharge $\mathbf{q}(x,y)$, connected to discrete 'channels', with cross-sectional area $S(s)$ and discharge $Q(s)$, that are arranged along the edges and diagonals of the rectangular computational grid ($s$ denotes distance along a channel; see Supplementary material). The water pressure in the sheet, $p_w$, as with the quantities $h$ and $\mathbf{q}$, is treated as an average over some representative area of the bed, and is assumed to be continuous with the pressure in the channels.

The discharge in sheet and channels are given by

$$\mathbf{q} = -\frac{Kh^3}{\rho_w g}\nabla\phi \quad \text{and} \quad Q = -K_c S^{5/4}\left|\frac{\partial\phi}{\partial s}\right|^{-1/2}\frac{\partial\phi}{\partial s}, \tag{3}$$

where $\phi(x,y) = \rho_w g b(x,y) + p_w(x,y)$ is the hydraulic potential, $\rho_w$ is the water density, $Kh^3$ represents an effective hydraulic transmissivity, and $K_c$ is a turbulent flow coefficient. Channel cross-sectional area $S$ evolves according to

$$\frac{\partial S}{\partial t} = \frac{\rho_w}{\rho_i}M - \frac{2A}{n^n}S|N|^{n-1}N, \tag{4}$$

where $M$ is the melting rate of the channel walls, and the final term represents the counteracting creep of the ice due to the effective pressure ($A$ and $n$ are Glen's law parameters).

There are two alternative models for the sheet: a 'cavity' model and a 'poroelastic' model. In the cavity model $h = h_{cav}$ represents the size of individual cavities and orifices (Schoof et al., 2012), and evolves according to

$$\frac{\partial h_{cav}}{\partial t} = \frac{\rho_w}{\rho_i}m + U_b(h_r - h_{cav})/l_r - \frac{2A}{n^n}h_{cav}|N|^{n-1}N, \tag{5a}$$

where $m$ is the basal melting rate, $h_r$ and $l_r$ are bed roughness height and length scales, respectively, and $U_b$ is the sliding speed. The second term here represents the opening of cavities due to ice sliding over bed roughness and the third term represents creep closure of the cavity roofs. In the poroelastic model the sheet thickness $h = h_{el}$ is directly related to the water pressure or effective pressure by, e.g.

$$h_{el} = h_c\left(\frac{p_w}{p_i}\right)^{\gamma}, \tag{5b}$$

for a critical layer depth $h_c$ and exponent $\gamma$; other functional forms are possible (cf. Flowers and Clarke, 2002).

Energy considerations determine the basal melting rates $m$ and $M$. The heat sources that give rise to melting are the net conductive flux $G$ (geothermal less conductive loss through the ice), the frictional heating $\boldsymbol{\tau}_b \cdot \mathbf{u}_b$, and the dissipative heating due to water flow, $|\mathbf{q}\cdot\nabla\phi|$ or $|Q\partial\phi/\partial s|$. Because the latter is responsible for channel formation (Walder, 1986; Kamb, 1987; Schoof, 2010), I account for dissipative heating only within the channels, adding a small contribution from the sheet to represent the initial perturbation from which the channel emerges (Hewitt et al., 2012). That leaves the conductive and frictional heating to account for the distributed melting rate, so

$$m = \frac{G + \boldsymbol{\tau}_b \cdot \mathbf{u}_b}{\rho_w L} \quad \text{and} \quad M = \frac{|Q\partial\phi/\partial s| + \lambda_c|\mathbf{q}\cdot\nabla\phi|}{\rho_w L}, \tag{6}$$

where $L$ is the latent heat and $\lambda_c$ is an incipient channel width (representing the length scale over which ice melting contributes to initiating a channel). The pressure dependence of the melting point has been neglected for simplicity.

Finally, mass conservation is expressed as

$$\frac{\partial h}{\partial t} + \nabla\cdot\mathbf{q} + \left[\frac{\partial S}{\partial t} + \frac{\partial Q}{\partial s}\right]\delta(\mathbf{x}_c) + \frac{\partial V}{\partial t}\delta(\mathbf{x}_m) + \frac{\partial \Sigma}{\partial t} = m + M\delta(\mathbf{x}_c) + R\delta(\mathbf{x}_m), \tag{7}$$

where the delta functions apply along the (linear) positions of the channels, $\mathbf{x}_c(s)$, and the (point) positions of the moulins, $\mathbf{x}_m$. $R$ is

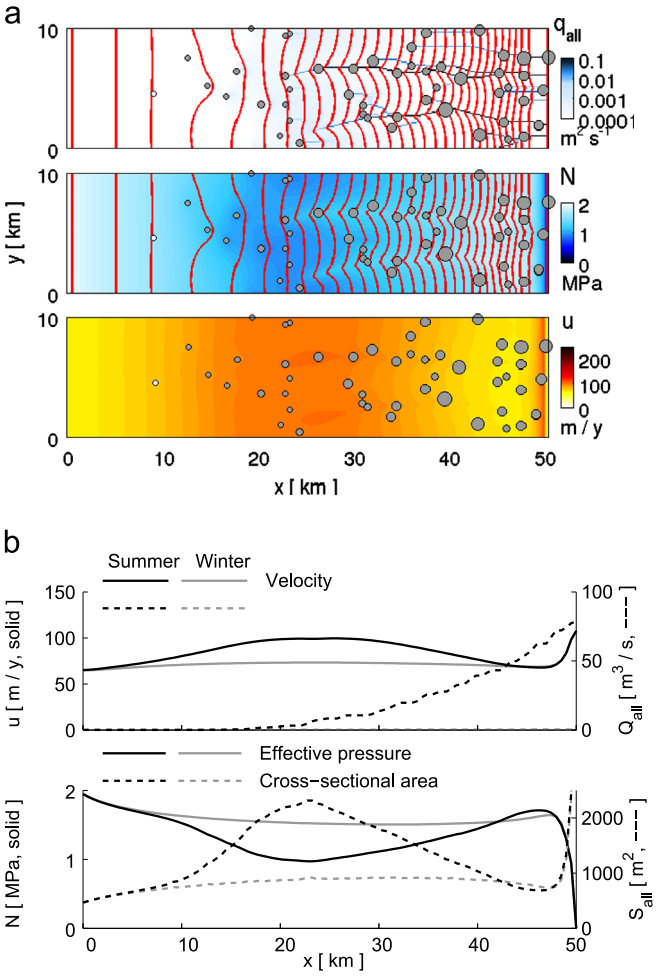


**Fig. 2.** (a) Solution for a hypothetical steady state for summer melting showing subglacial water discharge $q_{all}$, effective pressure $N$, and surface ice velocity $u$ (the discharge $q_{all}$ includes flow in the channels, which is spread out over the width of the grid cells for visualization purposes). The surface input is $r = \max\{0, r_m - r_s(s - s_m)\}$ with $r_m = 25$ mm d$^{-1}$ (cf. Fig. 1). Filled circles represent the magnitude of inflow to the moulins, red lines are contours of subglacial water pressure (decreasing to the right). (b) Width-averaged surface velocity $u$ and effective pressure $N$, and width-integrated water discharge $Q_{all}$ and area $S_{all}$ compared to their background values for the winter solution with no surface runoff (grey). Parameter values are in Table 1. (For interpretation of the references to colour in this figure caption, the reader is referred to the web version of this article.)

the forcing input into the moulins, and $V$ represents the volume of water stored in the moulins, a function of the hydraulic head $H_w = p_w/\rho_w g$ approximated by $V = S_m H_w$, where $S_m$ is their average cross-sectional area. The term $\Sigma$ represents possible additional water storage in connected void space within the ice sheet (Harper et al., 2010; Bartholomaus et al., 2011); it is also assumed to vary linearly with hydraulic head and is given by $\Sigma = \sigma H_w$, where $\sigma$ is the connected void fraction of the ice.

As for the basal sliding law, it is not known what the correct equations are, let alone the parameters, to model the drainage system. A brief comparison with other published models is given in the Appendix, and there is more discussion of this model's validity in Section 4.

### 2.4. Boundary conditions

Boundary conditions in the $y$-direction are periodic. For the ice flow, the left hand upstream margin has a prescribed basal velocity and the right hand margin has zero deviatoric stress. For the drainage system, there is no inflow of water from the upstream margin, and atmospheric pressure is applied at the right hand margin. These boundary conditions remain unchanged for all the calculations in this paper, as do the positions of the moulins. The numerical procedure is described in the Supplementary material.

### 2.5. Steady-state melting and winter reference case

Fig. 2 shows a steady state for 'summer' melting, and compares this to a reference 'winter' state for which there is no surface input (a small amount of water is still produced due to the geothermal and frictional heating $m$). It is unlikely that either of these steady states are ever actually realized in the course of an annual cycle; it takes over two years of sustained input to evolve from one to the other (see below). The 'standard' model shown here uses the simpler sliding law (2a) with $p = q = 1$, and the cavity version of the sheet, $h = h_{cav}$. Parameter values have been chosen in order to match in a very general sense the types of behaviour that have been observed. Some parameters allow for little freedom, but others are poorly constrained; the values used are given and discussed in the Appendix (Table 1). Parameters for the ice flow are such that most of the surface motion results from basal sliding.

Initial conditions for the following calculations are the winter reference state shown in Fig. 2(b). In all cases, simulations are run for two consecutive years, the second of which is shown.

## 3. Results

### 3.1. An annual cycle

Fig. 3 shows an example of the response to the melting input shown in Fig. 1. Fig. 3a shows snapshots of the drainage system and the surface velocity of the ice through the summer. Averages across the width of the domain are taken at each instant and are shown as a function of time in Fig. 3b, which gives an overall picture of the evolution of drainage system and ice motion.

This example demonstrates some of the expected behaviour mentioned in the introduction. The drainage system expands upglacier with the melt region, and the resulting high pressures cause a similar upward-propagating increase in velocity (see Fig. 3b). Close to the margin, water flow gradually melts channels that connect the moulins and lead to a slow reduction in water pressure and ice velocity (channels grow at the expense of the distributed cavities, so are also marked by a reduction in the overall drainage system area $S_{all}$, Fig. 3b). The water flow is not as concentrated as in Fig. 2; this is because the input to the moulins initially forces them to be at a higher pressure than their surroundings so that water spreads in all directions over the bed (cf. Gulley et al., 2012). The season is simply not long enough for the flow to focus into a well-defined channel network as in Fig. 2, when channels operate as low pressure catchments that draw in surrounding water.

Changes in ice velocity largely follow the pattern of pressure changes, but are smoothed out by the membrane stresses on a length scale several times the ice thickness. Pressure changes upstream of the melting region are negligible and the velocity change seen there in Fig. 3b is the result of longitudinal coupling to the ice lower downstream (Price et al., 2008).

### 3.2. An annual cycle with diurnal oscillations

To compare different simulations I now consider time series for the four 'stake' locations A–D shown in Fig. 1, at distances 5, 15, 25 and 35 km from the margin.

Fig. 4 compares the above result with an example in which the same seasonal melt input is modulated by diurnal oscillations that

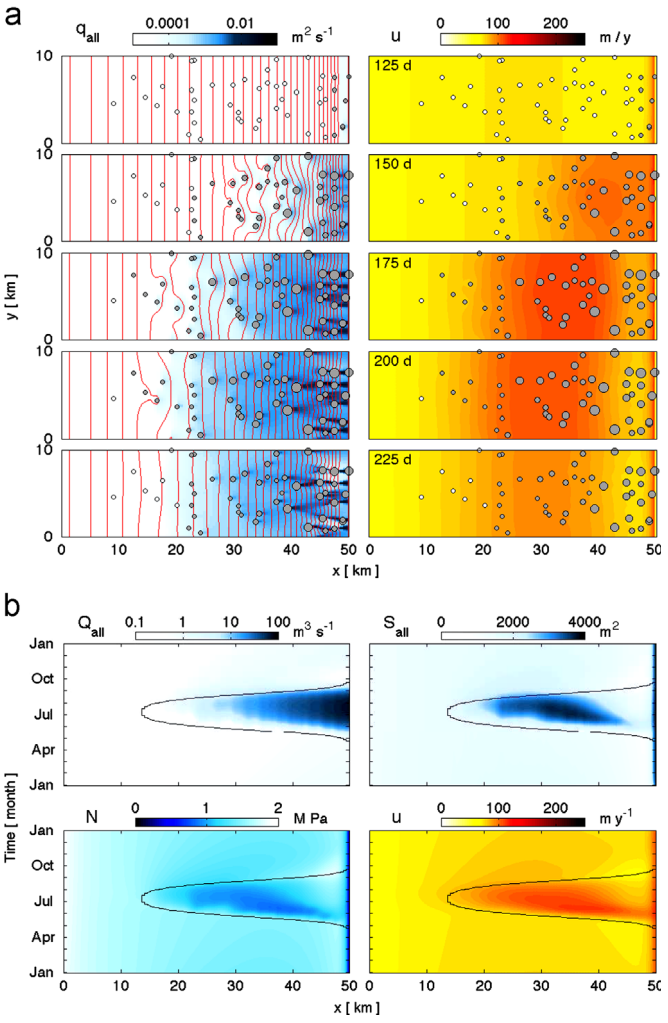


**Fig. 3.** (a) Snapshots of subglacial water discharge $q_{all}$ (left) and surface velocity $U$ (right) during an annual cycle at the times indicated by arrows in Fig. 1b. Filled circles represent the magnitude of inflow to the moulins, open circles show the locations of moulins with no inflow, and red lines are contours of subglacial water pressure. Surface input $r$ is given by the expression in Fig. 1 with $r_m = 25$ mm d$^{-1}$. Parameter values are in Table 1. (b) Width-integrated subglacial water discharge $Q_{all}$ and area $S_{all}$, and width-averaged effective pressure $N$ and ice surface velocity $u$ as a function of time on the $y$-axis. Black curves denote the extent of the melting region, where $r > 0$. (For interpretation of the references to colour in this figure caption, the reader is referred to the web version of this article.)

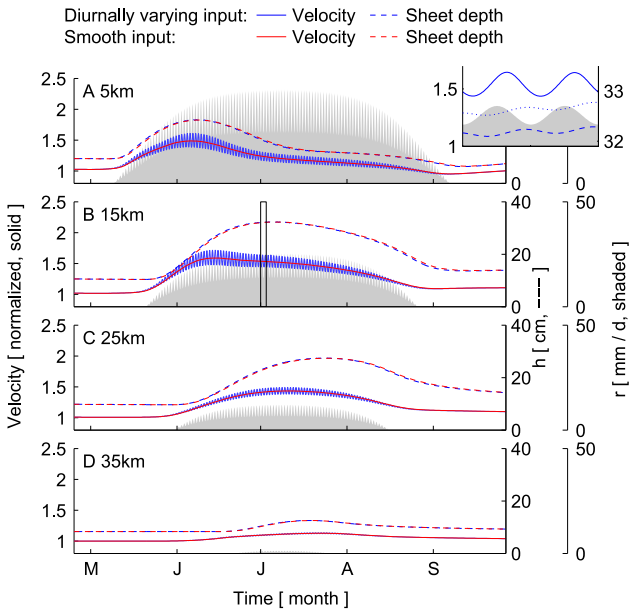


**Fig. 4.** Surface velocity (solid blue, normalized by the reference winter values), drainage system depth $h$ (dashed blue), and surface input $r$ (shaded), at positions A–D in Fig. 1. Melt input is as in Fig. 1, with $r_m = 25$ mm d$^{-1}$, modulated by a diurnal sinusoid with 30% amplitude (*i.e.* $r$ is multiplied by $(1-0.3\cos 2\pi t/t_d)$ where $t_d = 1$ d). Red lines show the equivalent case without the diurnal oscillations. The insets shows a close-up of stake B during the two day window shown by the vertical box; the additional dotted lines show the anticipated surface motion assuming changes in $h$ are propagated through the ice column. (For interpretation of the references to colour in this figure caption, the reader is referred to the web version of this article.)

have amplitude 30% about the mean. The general behaviour is essentially the same, but with diurnal velocity variations superimposed. Larger variations in input naturally lead to larger amplitude pressure and velocity fluctuations, and result in a slight increase in the annual mean velocity. This increase is due to the non-linearity of the sliding law (1), which results in a higher sensitivity of the sliding speed to low effective pressures.

It should be noted that the amounts of water storage in void space and moulins, $\Sigma$ and $V$, controlled by the parameters $\sigma$ and $S_m$, have a strong influence on both the amplitude and timing of diurnal variations. The more storage, the more damped are the pressure and velocity variations and the greater the delay relative to the melt signal. If there is no storage, either englacially or in the moulins, then the velocity peak is coincident with the peak in melt input and with the greatest rate of increase of sheet depth. In the example shown, with $\sigma = 10^{-4}$ and $S_m = 10$ m$^2$, the velocity peak is delayed by roughly 2 h (see the inset).

Variations of water sheet depth $h$ can be expected to translate to similar vertical motion of the ice surface, as is sometimes measured in GPS surveys. Additional surface motion results from convergence or divergence of ice flow, and the dotted lines in the inset to Fig. 4 show the expected surface motion after correcting for that (e.g. Howat et al., 2008). The divergence dominates the long-term trend, but has little diurnal contribution. In any case, diurnal variations in uplift are small, no more than a few mm, which may be hard to detect in the field (on average, of course, uplift variations should be no larger than variations in the input).

### 3.3. *Different versions of the model*

Fig. 5 shows the same annual cycle with diurnal oscillations using two variants to the standard model. In Fig. 5a, sliding law (2a) is replaced with (2b), with parameters chosen to give a similar magnitude and range of sliding velocity. The general behaviour

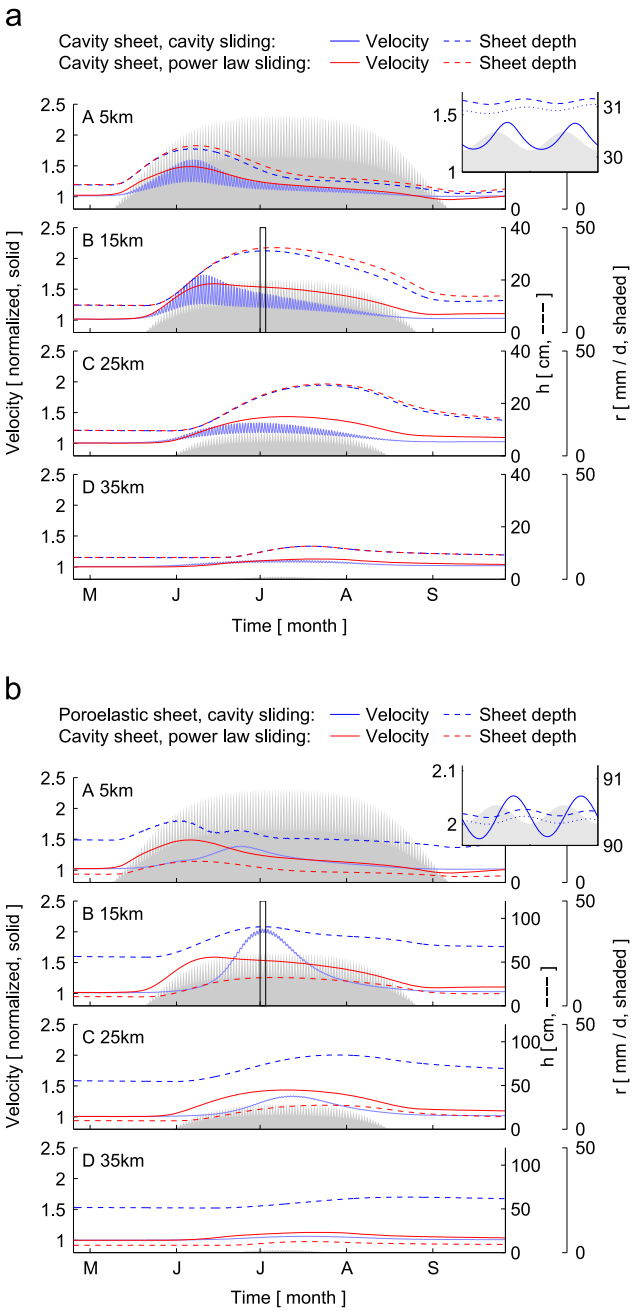


**Fig. 5.** The same as Fig. 4, but using the cavity sliding law (2b) rather than the power law (2a). Panel (a) has the cavity sheet (5a) and panel (b) the poroelastic sheet (5b). Red lines here are identical to those in Fig. 4 for comparison to that solution. (For interpretation of the references to colour in this figure caption, the reader is referred to the web version of this article.)

is not significantly different, though there are some slight differences, notably the larger amplitude of the diurnal velocity cycles. The same calculation using sliding law (2a) but with $p = q = 1/3$ also yields similar results.

Fig. 5b makes use of the poroelastic version of the water sheet $h = h_{el}$ (5b) instead of the cavity equation (5a). There are more significant differences in this case; in particular, peak velocities occur later in the year and there is a much weaker diurnal signal. In that version of the model, the highest water pressure occurs at the same time as maximum depth of the water sheet, $h$, so velocity variations should be roughly in phase with changes in $h$, rather than with $\partial h/\partial t$ as in the cavity model. This correlation is not particularly clear in Fig. 5b because longitudinal coupling means the velocity responds to pressure changes over a wider area, and

the seasonal peak in pressure occurs progressively later up glacier. On the diurnal timescale, the fact that water pressure is tied to sheet depth heavily dampens the oscillations compared to the cavity sheet; a similar lack of diurnal variability was found by Pimentel and Flowers (2011).

### 3.4. Varying the melt input

The primary goal of this study is to calculate the expected influence of more, or less, surface melting on the mean annual ice velocity. This is investigated using the smoothly varying input from Fig. 1 without diurnal modulation (the preceding results suggest such modulation may generate diurnal variability but without hugely altering the mean). The same calculations as in Fig. 3 are performed for different values of the peak melting rate $r_m$, and the results are shown in Fig. 6. Increasing $r_m$ has the effect of increasing both the magnitude and the spatial extent of the melting.

The results show a general increase in the mean annual velocity with increased melting. The rate of increase varies strongly in space, however. Close to the margin, larger melting rates lead to a higher peak velocity during the spring followed by a more dramatic slow-down as an efficient drainage system is established more quickly. This early summer increase and late summer decrease largely cancel out and there is little change in the annual mean. Further from the margin, higher velocities are sustained throughout the year in response to the higher input. The greatest increases in annual mean velocity occur near the upper reaches of the melting region where the relatively small increase in melt water nevertheless overwhelms the capacity of the drainage system and leads to higher water pressure throughout the summer.

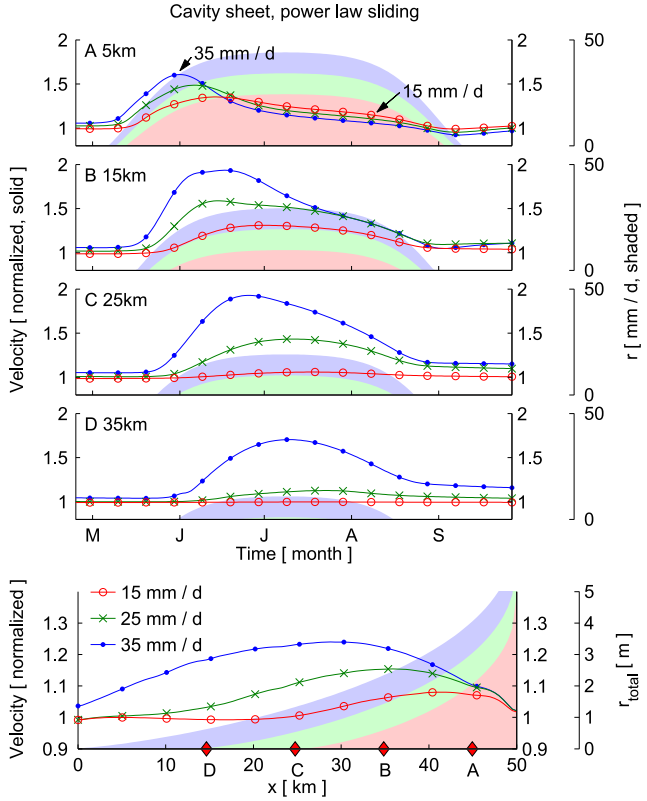


**Fig. 6.** Surface velocity time series at positions A–D for different melting rates. Coloured shading shows the local melting rate $r$ and labels indicate the value of $r_m$ which corresponds to the peak melting rate at 500 m elevation. The lower panel shows the annually averaged velocity profile along the central flowline through points A–D, with shading showing the total annual melt input $r_{total}$. (For interpretation of the references to colour in this figure caption, the reader is referred to the web version of this article.)

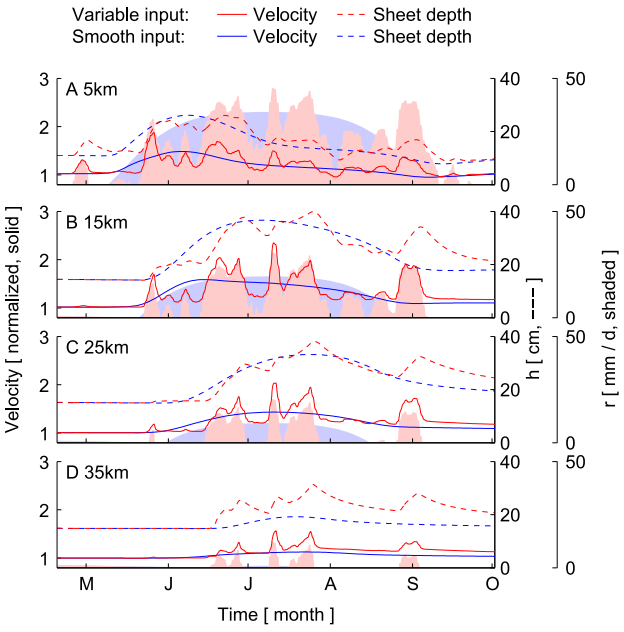


**Fig. 7.** Response to a synthetically generated time series of melting (red) compared to that for the idealized melt input in Fig. 1 (blue). Solid lines show the normalized surface velocity at positions A–D, dashed lines show the water sheet depth $h$, and the shading shows the melt input, given by $r = \max\{0, \hat{r}(t) - r_s(s - s_m)\}$, where $\hat{r}(t)$ is modified from an annual temperature record. (For interpretation of the references to colour in this figure caption, the reader is referred to the web version of this article.)

### 3.5. A more realistic input

A reasonable query of these results is whether one can expect the response to these idealized seasonal forcings to bear any resemblance to the real situation, when meteorological conditions give rise to a much more variable input. To investigate this issue rather crudely, Fig. 7 shows a calculation using a time series of melt input generated synthetically from a temperature record, and compares the result with the idealized input that has the same total quantity of melt over the year.

Rapid increases in melting inevitably lead to sudden speed-up events that are absent in the smoothly varying results seen before. The net result of these appears to be an increase in the average speed over the course of the year, but the difference is not huge. It is instructive to note, for instance, that peak velocities are much higher with the more variable input, but there are also periods of low input when the velocity decreases significantly, almost to its background value.

It is reassuring to see some typically observed behaviour being reproduced by the model: speed-up correlates with rapid increases in water storage that are followed by a slower collapse of the drainage system (Bartholomaus et al., 2008); the highest velocity near the margin occurs at the beginning of summer and later increases in melting are accommodated more easily, whereas further inland the highest velocities occur later (Bartholomew et al., 2010). The rather remarkable correlation between melt input and ice velocity at position B occurs despite no *direct* link between the two in the model.

## 4. Discussion

### 4.1. Comparison with observations

The outputs of this model are broadly consistent with observations from the land-terminating margins in Greenland. Typical

measurements in the ablation zone find summer speeds around 10–50% above the winter average, with the highest velocities generally occurring early in the summer (Joughin et al., 2008; Sundal et al., 2011). Diurnal velocity variations up to around 100% of the mean, and sometimes more, have been observed in a number of locations (Shepherd et al., 2009; Hoffman et al., 2011; Bartholomew et al., 2012).

Diurnal and other short-term fluctuations provide useful information with which to constrain the model. It is most commonly observed that peak velocities are correlated with the rate of change of subglacial water storage (inferred from GPS uplift, Howat et al., 2008 or from runoff modelling, Bartholomaus et al., 2008), rather than with water storage itself. As alluded to earlier, that behaviour is more consistent with the cavity version of the sheet in (5a) rather than the elastic version in (5b). Coupled with the more obvious physical basis for (5a), I am therefore led to favour that version of the model.

The amplitude and timing of diurnal velocity changes also place constraints on the amount of englacial storage, controlled by the parameter $\sigma$; if there is too much storage, small adjustments in the englacial water table absorb all of the input fluctuations, with more subdued velocity, pressure, and uplift response as a result. Spatial variations of storage likely contribute to different amounts of diurnal variability in different locations.

An obvious extension of this work is to use specific observations to test how successful the model is. In addition to measurements of surface melting, velocity and uplift, further constraints could be provided by observations of water pressure in boreholes or moulins, of proglacial discharge, and of dye and chemical tracing experiments.

### 4.2. Effect of topography

The geometry of the channel network depends on the position of the moulins, as it intuitively must (Fig. 2). It is also sensitive to the structure of the numerical grid. This is probably not a major issue for this study since the fact that the channels are there at all is far more important than their exact position and orientation. In reality, one anticipates that surface and basal topography should guide the location of the channels and an unstructured grid of potential channel segments may be important in allowing for this in the model (Werder et al., submitted for publication).

Larger scale routing of the water into supraglacial and subglacial valleys may play a role in controlling the spatial pattern of velocity changes (Palmer et al., 2011). This is not observed here because the moulins are close enough together that membrane stresses smooth out any variations (in fact, this model does not accurately resolve short length scale velocity variations; see discussion in the Supplementary material).

### 4.3. Channel behaviour

The conduit theory is the most standard model for subglacial water flow and as such, Eqs. $(3)_2$ and (4) are perhaps on the firmest footing. The issue of how small channels initiate is debatable, however. The term $\lambda_c$ in $(6)_2$ must essentially be viewed as a control parameter for how easily a channel begins to grow; larger values result in more rapid growth of channels during spring, reducing both the maximum and the average velocity (see the Appendix). An alternative way to control the size of small channels is to add a small 'cavity opening' term to (4) (Schoof, 2010). For some authors, the issue of channel initialization manifests itself in the initial conditions for the numerical model (Pimentel and Flowers, 2011), or is circumvented by imposing a minimum channel size (Colgan et al., 2012).

The channels in this model invariably shrink over winter and are all extremely small by the start of the following melt season ($S \lesssim 20\ \mathrm{cm}^2$). The growth of a network thus starts afresh each year. In reality it seems quite plausible that some larger vestige of the previous years' channels does persist, particularly if those channels have eroded their bed and are flushed of impermeable sediments (Gulley et al., 2012). Any pre-existing permeable pathways would hasten the establishment of a more efficient drainage system that expands further up glacier, and would lead to a more significant slowdown below the reference winter velocity at the end of summer and beginning of winter.

### 4.4. Sheet behaviour

The conductivity parameter $K$ is probably the least constrained of the parameters in this model; the value chosen gives an effective hydraulic conductivity of around $0.02\ \mathrm{m\ s^{-1}}$. A smaller value yields a higher pressure over the winter and during the initial spring event, but also accelerates the growth of channels and the subsequent pressure reduction (see the Appendix). If anything, I suggest that a smaller value of $K$ may be more appropriate, but that leads to predictions of excessively high water pressure in spring that are currently problematic (see below).

The feedback of the sliding speed causing cavities to open in (5a) plays an important role in enabling the sheet to accommodate the inflow of water at the start of the season (Bartholomaus et al., 2011). Without this increase in cavity opening, higher pressures are predicted and a de-coupled calculation of the ice flow without the feedback gives erroneously large velocities.

In contrast to the winter shrinkage of the channels, the distributed system has more memory of the melt season and does not generally return to the original reference state at the end of the year. Depending on the choice of parameters, the sheet may absorb some of the summer melt water and become larger (and higher pressured), or it may be flushed out by the growth of the channels in the summer and thus contain less water than it would had the melting season never happened. This long-term memory is the reason why the first year of simulation is not shown; running the calculations for longer still might be better, but the difference after two years appears minimal.

### 4.5. High water pressure

A significant deficiency of this model is its inability to deal with sudden large water inputs or with periods of extensive high water pressure. I have deliberately shown calculations in which the water pressure does not exceed the overburden (flotation) level $p_i$ over a wide area, and this limits the parameter values for which the model gives sensible results. Large areas of negative effective pressure cause the ice velocity to increase almost without bound (without more variable topography, membrane stresses are ineffective at holding back the ice).

In reality, high water pressure may cause instantaneous uplift of the ice (Das et al., 2008) and this rapid creation of additional drainage space acts to alleviate the predicted high pressure. Schoof et al. (2012) suggested a method to account for this process, but the numerical method devised is prohibitively expensive. Pimentel and Flowers (2011) accounted for uplift using an elastic beam model, and Tsai and Rice (2010) modelled an individual lake drainage event as a hydrofracture along the ice-bed interface. It is possible that similar approaches might be extended to a two-dimensional model. Alternatively one can use the elastic version of the sheet to allow for a rapid increase of $h$ in response to negative effective pressure.

### 4.6. Sliding law

All the calculations in this paper assume that the relationship between basal velocity and shear stress is controlled by effective pressure. On that basis, it seems, a good deal of the observed behaviour can be reproduced using either of the friction laws (2a) or (2b), and there is little obvious reason to choose one or the other on this evidence. The parameters were chosen to demonstrate similar behaviour, however, and there are of course differences between these laws. The cavity version in (2b) becomes independent of the hydrology when the effective pressure is large, and also exhibits the bound $\tau_b \leq \mu_b N$. This form has the stronger theoretical basis, while the form in (2a) has the advantage of simplicity, involving fewer free parameters.

On the other hand, it is not clear that either of these relationships are really correct. Many observations of borehole water pressure on smaller glaciers do not find a simple correlation with ice speed (Hanson et al., 1998; Sugiyama and Gudmundsson, 2004; Harper et al., 2005; Howat et al., 2008; Fudge et al., 2009). This may be because borehole water pressures do not accurately represent the local average water pressure that is relevant for the sliding law. At the same time, it raises the awkward question of whether such an average is really meaningful. The conceptual basis of the model is that the drainage system can be described with a local average pressure that varies continuously in space; this assumes a certain degree of connectivity so that individual cavities are not all acting independently. It is quite possible, particularly during winter, that this picture is not a good one.

A related awkward inconsistency lies in the theoretical justification for the friction law (2b) (Fowler, 1986; Schoof, 2005; Gagliardini et al., 2007). At least for hard-bedded glaciers, this is based on *steady-state* calculations of basal cavitation; a more complicated version of (5a) is effectively solved to determine cavity size as a function of effective pressure, and thus calculate the basal drag. Since the *evolution* of cavity size is included in (5a) as an important component of the hydrological model, the use of a steady-state sliding law puts us on rather shaky ground.

Future work must establish a more self-consistent parameterization of hydraulically controlled sliding. This may include an additional state variable to represent the extent of bed separation that evolves in time (and is related to the cavity size encoded in $h_{cav}$). The combination of this state, and the effective pressure, then controls the friction law (e.g. Iken, 1981).

Given these observational and theoretical issues, the appropriateness of sliding laws (2a) or (2b), for the practical purposes of modelling on the ice sheet scale, remains uncertain. For the time being, the most reliable predictions of ice flow will continue to use the empirical approach of fitting a spatially variable parameter $\beta^2$ in the friction law $\boldsymbol{\tau}_b = \beta^2 \mathbf{u}_b$ (fitting to annual mean velocities, if possible, so that any summer speed-up is accounted for). At the same time, it is important to explore the theoretical implications of hydrologically coupled sliding laws that allow the impact of all potential feedbacks to be established.

## 5. Conclusions

I have presented a model to describe the drainage system beneath an ice sheet margin and its influence on ice motion. The model predicts generally increased ice speeds throughout the melt season, with the largest speeds usually occurring in early summer when there is the greatest imbalance between melt water runoff and drainage system capacity. The behaviour is broadly consistent with observations of melt-induced seasonal speed-up in Greenland.

The model suggests that increased quantities of surface melting lead to an increase in the average speed of the ice over the year, except perhaps very close to the margin. The establishment of an efficient channelized drainage system during late summer helps to offset a larger speed-up in early summer, but is unlikely to cause any significant reduction in the average speed.

Accounting for short-term variability in the input yields large velocity fluctuations that result in a slight increase in the mean. The solutions also suggest that observations of *maximum* summer speed-up do not give a good indication of the seasonal average. The long-term average velocity is the relevant quantity affecting the ice sheet's mass balance.

Finally, I have discussed some issues with current sliding laws. Future studies should critically assess the relationship between the implicitly average water pressure that is invoked in the sliding law, and the point measurements obtained from boreholes. Theoretical improvements will lead to a more consistent treatment of the drainage system and sliding law.

## Acknowledgements

My thanks to M. Werder, G. Flowers and C. Schoof for ongoing and stimulating discussions on the subject of subglacial drainage.

## Appendix A. Relation to other models of basal hydrology

The hydrology model in Section 2, incorporating the cavity version of the sheet in (5a), is essentially the same as that suggested by Hewitt et al. (2012), though without concern for the pressure bounds discussed there. An extension of these models to an unstructured finite element mesh is described by Werder et al. (submitted for publication). Without the distributed sheet, and instead including an additional 'cavity opening' term in (4), the model is equivalent to the network of conduits used by Schoof (2010). Creyts and Schoof (2009) describe a sheet that evolves according to a similar equation to (5a) but with a more complicated expression for creep closure.

Flowers and Clarke (2002) use the poroelastic version of the sheet (5b) with $\gamma = 2/7$, with a slightly different expression for the conductivity in $(3)_1$, and Flowers et al. (2004) and Pimentel and Flowers (2011) combine the sheet with channels in one dimension. A difference in those models is the allowance for different water pressures in sheet and channel, with water exchange proportional to the pressure difference (here, that exchange is implicitly accounted for by the delta functions in (7); this model may be thought of as the limit of large exchange coefficient $\chi$ in that model).

The model of Le Brocq et al. (2009) uses a sheet with $(3)_1$, setting water pressure equal to ice pressure in the potential $\phi$, so that the mass conservation equation (7) becomes a hyperbolic equation for $h$ (an equation like (5) is not needed in that case, except perhaps to infer the neglected effective pressure). Johnson and Fastook (2002) take a similar approach but use an equivalent of (5b) to relate the effective pressure to $h$, effectively adding a diffusive term to (7). Indeed, a number of other models involve a diffusion equation for the water depth (Bueler and Brown, 2008; Sayag and Tziperman, 2008; van Pelt and Oerlemans, 2012); that results from a linearization of the conservation equation (7) when the poroelastic relationship (5b) or similar is used to relate effective pressure to $h$, and the surface slope of the ice is ignored.

## Appendix B. Parameter values

Values of the parameters used are given in Table 1. The value of $A$ is appropriate for ice at 0 °C (Paterson, 1994) with $n = 3$, and the value of $\overline{A}$ (see Supplementary material) is taken to be 10 times smaller to roughly account for the effect of colder ice near the surface. The value

**Table 1**
Standard values used for the model parameters. The standard model uses sliding law (2a) with $p=q=1$ and the cavity sheet (5a).

| | |
|---|---|
| $\rho_w$ | 1000 kg m$^{-3}$ |
| $\rho_i$ | 910 kg m$^{-3}$ |
| $g$ | 9.8 m s$^{-2}$ |
| $n$ | 3 |
| $A$ | $6.8\times10^{-24}$ Pa$^{-3}$ s$^{-1}$ |
| $\overline{A}$ | $6.8\times10^{-25}$ Pa$^{-3}$ s$^{-1}$ |
| $p$ | 1[a] |
| $q$ | 1[a] |
| $\mu_a$ | $3.2\times10^{4}$ s m$^{-1}$[a] |
| $\mu_b$ | 0.16 |
| $\lambda_b$ | 1 m |
| $L$ | $3.35\times10^{5}$ J kg$^{-3}$ |
| $G$ | 0.063 W m$^{-2}$ |
| $S_m$ | 10 m$^2$ |
| $\sigma$ | $10^{-4}$ |
| $K_c$ | 0.1 m s$^{-1}$ Pa$^{-1/2}$ |
| $\lambda_c$ | 20 m |
| $K$ | 2 m$^{-1}$ s$^{-1}$[b] |
| $h_r$ | 0.5 m |
| $l_r$ | 5 m |
| $h_c$ | 1 m |
| $\gamma$ | 1 |

[a] $\mu_a=6.8\times10^{4}$ Pa$^{2/3}$ s$^{1/3}$ m$^{-1/3}$ when using $p=q=1/3$.
[b] $K=0.05$ m$^{-1}$ s$^{-1}$ when using the poroelastic sheet.

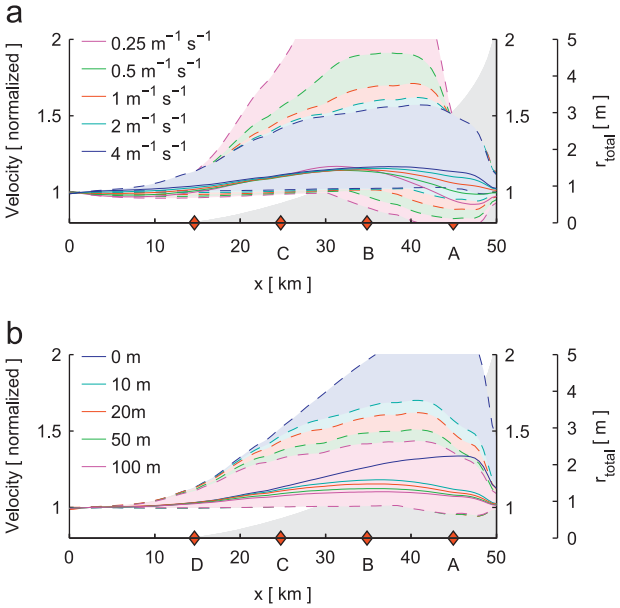


**Fig. 8.** Annual mean velocity profiles (solid), and ranges (dashed), using different values of (a) sheet conductivity parameter $K$ and (b) channel-initiating width $\lambda_c$ ($\lambda_c=0$ means there are no channels at all). These calculations are comparable to those in figure 6. They are for the standard melting input as in Fig. 1, with $r_m=25$ mm d$^{-1}$, and all other parameters take their standard values in Table 1. (For interpretation of the references to colour in this figure caption, the reader is referred to the web version of this article.)

$\mu_a$ in (2a) is chosen so as to give a sliding speed on the order of 60 m yr$^{-1}$ for the typical driving stress 100 kPa. Values of $\mu_b$ and $\lambda_b$ are chosen to give similar rates using the cavity law (2b). $G$ is taken as an average Greenland geothermal heat flux, neglecting conductive heat loss into the ice. The moulin area $S_m$ corresponds to a radius of 1.8 m. The value of $K_c$ is consistent with a Darcy–Weisbach law with friction factor $f_R=0.2$ in a semicircular conduit, for which $K_c=2^{5/4}\pi^{1/4}/(\pi+2)^{1/2}\rho_w^{1/2}f_R^{1/2}$ (e.g. Clarke, 2003).

The value $\sigma=10^{-4}$ for connected void fraction is considerably less than used by some other authors for smaller glaciers (the models of Kessler and Anderson (2004) and Colgan et al. (2012) take $\sigma=0.01$, and that of Bartholomaus et al. (2011) has $\sigma=0.007$, while Bradford et al. (2009) estimate englacial water content between 1% and 2.5% for Bench Glacier and Huss et al. (2007) infer values between 0.1% and 10% for Gornergletscher). The storage term $\Sigma$ represents water that has a direct no-resistance connection to the bed; even if those larger values of void fraction are appropriate for a thick ice sheet, it seems highly unlikely that it is all well connected, and it might be better modelled as a separate englacial component (cf. Flowers and Clarke, 2002). Taking a much larger value for $\sigma$ gives severely damped diurnal oscillations and can also lead to chaotic looking flood events. An alternative interpretation of $\Sigma$ is as a relatively impermeable till aquifer; a 1 m thick layer of till with specific storage $10^{-4}$ m$^{-1}$ (Fountain and Walder, 1998) would give $\sigma=10^{-4}$.

Values of $h_r$ and $l_r$ are chosen as seemingly plausible length scales for bed roughness (similar values have been taken by Kessler and Anderson, 2004; Schoof, 2010; Bartholomaus et al., 2011). The conductivity constant $K$ is chosen mainly by trial in order to achieve realistic looking results. The value used, at the typical sheet depths $h\approx10$ cm, corresponds to an effective hydraulic conductivity $Kh^2$ of around 0.02 m s$^{-1}$, giving typical water velocities around 0.4 mm s$^{-1}$ for the average potential gradient; this is comparable to values used elsewhere (Pimentel and Flowers, 2011). It is much larger than conductivity values inferred for subglacial till, which range between $10^{-9}$ and $10^{-4}$ m s$^{-1}$ (Fountain and Walder, 1998). The effect of varying $K$ is shown in Fig. 8. That figure also shows the effect of the incipient channel width $\lambda_c$.

The critical sheet depth $h_c=1$ m for the elastic sheet (5b) is chosen as seeming reasonable (Pimentel and Flowers (2011) used $h_c=5$ m for Greenland, finding a higher value necessary than for an alpine glacier; Bueler and Brown (2008) and van Pelt and Oerlemans (2012) used a value of 2 m for their equivalent 'saturation thickness'). To preserve roughly the same effective conductivity for the larger values of $h\approx60$ cm, a smaller value of $K$ was used for the elastic sheet. $\gamma=1$ is chosen for its simplicity, despite empirical backing for the value $\gamma=2/7$ (Flowers and Clarke, 2002; the latter gives greater sensitivity of the water pressure to $h$, and I find it generally requires more careful tuning to generate realistic seeming pressures).

## Appendix C. Supplementary materials

Supplementary data associated with this article can be found in the online version at http://dx.doi.org.10.1016/j.epsl.2013.04.022.

## References

Alley, R.B., 1996. Towards a hydrological model for computerized ice-sheet simulations. Hydrol. Proc. 10, 649–660.
Bartholomaus, T.C., Anderson, R.S., Anderson, S.P., 2008. Response of glacier basal motion to transient water storage. Nat. Geosci. 1, 33–37.
Bartholomaus, T.C., Anderson, R.S., Anderson, S.P., 2011. Growth and collapse of the distributed subglacial hydrologic system of Kennicott Glacier, Alaska, USA, and its effects on basal motion. J. Glaciol. 57 (206), 985–1002.
Bartholomew, I., Nienow, P., Mair, D., Hubbard, A., King, M.A., Sole, A., 2010. Seasonal evolution of subglacial drainage and acceleration in a Greenland outlet glacier. Nat. Geosci. 3, 408–411.
Bartholomew, I., Nienow, P., Sole, A., Mair, D., Cowton, T., Palmer, S., Wadham, J., 2012. Short-term variability in Greenland Ice Sheet motion forced by time-varying meltwater drainage: implications for the relationship between subglacial drainage system behavior and ice velocity. J. Geophys. Res. 117, F03002.

Bindschadler, R., 1983. The importance of pressurized subglacial water in separation and sliding at the glacier bed. J. Glaciol. 28, 239–265.
Bougamont, M., Price, S., Christoffersen, P., Payne, A.J., 2011. Dynamic patterns of ice stream flow in a 3-D higher-order ice sheet model with plastic bed and simplified hydrology. J. Geophys. Res. 116.
Bradford, J.H., Nichols, J., Mikesell, T.D., Harper, J.T., 2009. Continuous profiles of electromagnetic wave velocity and water content in glaciers: an example from Bench Glacier, Alaska, USA. Ann. Glaciol. 50, 1–9.
Budd, W.F., Keage, P.L., Blundy, N.A., 1979. Empirical studies of ice sliding. J. Glaciol. 23, 157–170.
Bueler, E., Brown, J., 2008. Shallow shelf approximation as a "sliding law" in a thermomechanically coupled ice sheet model. J. Geophys. Res. 114.
Clarke, G.K.C., 2003. Hydraulics of subglacial outburst floods: new insights from the Spring–Hutter formulation. J. Glaciol. 49, 299–313.
Colgan, L., Rajaram, H., Anderson, R., Steffen, K., Philips, T., Joughin, I., Zwally, H.J., Abdalati, W., 2012. The annual glaciohydrology cycle in the ablation zone of the Greenland Ice Sheet: Part 1. Hydrology model. J. Glaciol. 57, 697–709.
Creyts, T.T., Schoof, C.G., 2009. Drainage through subglacial water sheets. J. Geophys. Res. 114.
Das, S.B., Joughin, I., Behn, M., Howat, I.M., King, M.A., Lizarralde, D., Bhatia, M.P., 2008. Fracture propagation to the base of the Greenland Ice Sheet during supraglacial lake drainage. Science 320, 778–781.
Flowers, G., Clarke, G.K.C., Björnsson, H., Pálsson, F., 2004. A coupled sheet-conduit mechanism for jökulhlaup propagation. Geophys. Res. Lett. 31.
Flowers, G.E., Clarke, G.K.C., 2002. A multicomponent coupled model of glacier hydrology 1. Theory and synthetic examples. J. Geophys. Res. 107.
Fountain, A.G., Walder, J.S., 1998. Water flow through temperate glaciers. Rev. Geophys. 36, 299–328.
Fowler, A.C., 1986. A sliding law for glaciers of constant viscosity in the presence of subglacial cavitation. Proc. R. Soc. Lond. A 407, 147–170.
Fowler, A.C., Johnson, C., 1996. Ice-sheet surging and ice-stream formation. Ann. Glaciol. 23, 68–73.
Fudge, T.J., Harper, J.T., Humphrey, N.F., Pfeffer, W.T., 2009. Rapid glacier sliding, reverse ice motion and subglacial water pressure during an autumn rainstorm. Ann. Glaciol. 50, 101–108.
Gagliardini, O., Cohen, D., Råback, P., Zwinger, T., 2007. Finite-element modeling of subglacial cavities and related friction law. J. Geophys. Res. 112.
Gulley, J.D., Grabiec, M., Martin, J.B., Jania, J., Catania, G., Glowacki, P., 2012. The effect of discrete recharge by moulins and heterogeneity in flow-path efficiency at glacier beds on subglacial hydrology. J. Glaciol. 58, 926–940.
Hanson, B., Hooke, R.L., Grace, E.M., 1998. Short-term velocity and water-pressure variations down-glacier from a riegel, Storglaciären, Sweden. J. Glaciol. 44, 359–367.
Harper, J.T., Bradford, J.H., Humphrey, N.F., Meierbachtol, T.W., 2010. Vertical extension of the subglacial drainage system into basal cervasses. Nature 467, 579–582.
Harper, J.T., Humphrey, N.F., Pfeffer, W.T., Fudge, T.J., O'Neel, S., 2005. Evolution of subglacial water pressure along a glaciers length. Ann. Glaciol. 40, 31–36.
Hewitt, I.J., 2011. Modelling distributed and channelized subglacial drainage: the spacing of channels. J. Glaciol. 57, 302–314.
Hewitt, I.J., Schoof, C., Werder, M.A., 2012. Flotation and open water flow in a model for subglacial drainage. Part II: channel flow. J. Fluid Mech. 702, 157–187.
Hoffman, M.J., Catania, G.A., Neumann, T.A., Andrews, L.C., Rumrill, J.A., 2011. Links between acceleration, melting, and supraglacial lake drainage of the western Greenland Ice Sheet. J. Geophys. Res. 116 (F4), http://dx.doi.org/10.1029/2010JF001934.
Howat, I.M., Tulaczyk, S., Waddington, E., Björnsson, H., 2008. Dynamic controls on glacier basal motion inferred from surface ice motion. J. Geophys. Res. 113, http://dx.doi.org/10.1029/2007JF000925.
Huss, M., Bauder, A., Werder, M., Funk, M., Hock, R., 2007. Glacier-dammed lake outburst events of Gornersee, Switzerland. J. Glaciol. 53, 189–200.
Iken, A., 1981. The effect of the subglacial water pressure on the sliding velocity of a glacier in an idealized numerical model. J. Glaciol. 27, 407–421.
Johnson, J., Fastook, J.L., 2002. Northern hemisphere glaciation and its sensitivity to basal melt. Quat. Int. 95–96, 65–74.
Joughin, I., Das, S.B., King, M.A., Smith, B.E., Howat, I.M., Moon, T., 2008. Seasonal speedup along the Western flank of the Greenland Ice Sheet. Science 320, 781–783.
Kamb, B., 1987. Glacier surge mechanism based on linked cavity configuration of the basal water system. J. Geophys. Res. 92, 9083–9100.
Kessler, M.A., Anderson, R.S., 2004. Testing a numerical glacial hydrological model using spring speed-up events and outburst floods. Geophys. Res. Lett. 31.
Le Brocq, A., Payne, A.J., Siegert, M.J., Alley, R.B., 2009. A subglacial water-flow model for West Antarctica. J. Glaciol. 55, 879–888.
Palmer, S., Shepherd, A., Nienow, P., Joughin, I., 2011. Seasonal speedup of the Greenland Ice Sheet linked to routing of surface water. Earth Planet. Sci. Lett. 302, 423–428.
Paterson, W.S.B., 1994. The Physics of Glaciers. Butterworth-Heinemann.
Pimentel, S., Flowers, G.E., 2011. A numerical study of hydrologically driven glacier dynamics and subglacial flooding. Proc. R. Soc. A 467, 537–558.
Pimentel, S., Flowers, G.E., Schoof, C.G., 2010. A hydrologically coupled higher-order flow-band model of ice dynamics with a Coulomb friction sliding law. J. Geophys. Res. 115.
Price, S.F., Payne, A.J., Catania, G.A., Neumann, T.A., 2008. Seasonal acceleration of inland ice via longitudinal coupling to marginal ice. J. Glaciol. 54, 213–216.
Rignot, E., Kanagaratnam, P., 2006. Changes in the velocity structure of the Greenland Ice Sheet. Science 311, 986–990.
Sayag, R., Tziperman, E., 2008. Spontaneous generation of pure ice streams via flow instability: role of longitudinal shear stresses and subglacial till. J. Geophys. Res. 113.
Schoof, C., 2005. The effect of cavitation on glacier sliding. Proc. R. Soc. A 461, 609–627.
Schoof, C., 2010. Ice-sheet acceleration driven by melt supply variability. Nature 468, 803–806.
Schoof, C., Hewitt, I.J., Werder, M.A., 2012. Flotation and open water flow in a model for subglacial drainage. Part I: linked cavities. J. Fluid Mech. 702, 126–156.
Schoof, C., Hindmarsh, R.C.A., 2010. Thin-film flows with wall slip: an asymptotic analysis of higher order glacier flow models. Q. J. Mech. Appl. Math. 63, 73–114.
Shepherd, A., Hubbard, A., Nienow, P., King, M., McMillan, M., Joughin, I., 2009. Greenland ice sheet motion coupled with daily melting in late summer. Geophys. Res. Lett. 36.
Sole, A.J., Mair, D.W.F., Nienow, P.W., Bartholomew, I.D., King, M.A., Burke, M.J., Joughin, I., 2011. Seasonal speedup of a Greenland marine-terminating outlet glacier forced by surface melt-induced changes in subglacial hydrology. J. Geophys. Res. 116 (F3), F03014.
Sugiyama, S., Gudmundsson, G., 2004. Short-term variations in glacier flow controlled by subglacial water pressure at Lauteraargletscher, Bernese Alps, Switzerland. J. Glaciol. 50, 353–362.
Sundal, A.V., Shepherd, A., Nienow, O., Hanna, E., Palmer, S., Huybrechts, P., 2011. Melt-induced speed-up of Greenland ice sheet offset by efficient subglacial drainage. Nature 469, 521–524.
Tsai, V.R., Rice, J.R., 2010. A model for turbulent hydraulic fracture and application to crack propagation at glacier beds. J. Geophys. Res. 115.
van de Wal, R.S.W., Boot, W., van den Broeke, M.R., Smeet, C.J.P.P., Reijmer, C.H., Donker, J.J.A., Oerlemans, J., 2008. Large and rapid melt-induced velocity changes in the ablation zone of the Greenland ice sheet. Science 321, 111–113.
van Pelt, W.J.J., Oerlemans, J., 2012. Numerical simulations of cyclic behaviour in the Parallel Ice Sheet Model PISM. J. Glaciol.
Walder, J.S., 1982. Stability of sheet flow of water beneath temperate glaciers and implications for glacier surging. J. Glaciol. 28, 273–293.
Walder, J.S., 1986. Hydraulics of subglacial cavities. J. Glaciol. 32, 439–445.
Werder, M.A., Hewitt, I.J., Schoof, C., Flowers, G.E., Modeling channelized and distributed subglacial drainage in two dimensions, J. Geophys. Res., submitted for publication.

# Seasonal Changes in Ice Sheet Motion due to Melt Water Lubrication Supplementary Material

I. J. Hewitt

## 1. Model details

References to equations and figures in the main text are prefaced with an M, as in (M1) or figure M1.

### *1.1. Ice flow model*

The ice flow model is an approximation to the Stokes equations for an isothermal power-law fluid. The approximation can be derived asymptotically by assuming that the aspect ratio is small and the sliding speed is rapid (Schoof and Hindmarsh, 2010).

The constitutive law is approximated by ignoring horizontal derivatives in the vertical strain rates, by assuming in-plane strain rates are depth-independent, taking their values from the basal velocity $\mathbf{u}_b = (u_b, v_b)$, and by using an approximation for the effective viscosity for the in-plane stress components. Thus,

$$\tau_{xz} = \eta\frac{\partial u}{\partial z}, \quad \tau_{yz} = \eta\frac{\partial v}{\partial z}, \tag{1a}$$

$$\tau_{xx} = 2\tilde{\eta}\frac{\partial u_b}{\partial x}, \quad \tau_{yy} = 2\tilde{\eta}\frac{\partial v_b}{\partial y}, \quad \tau_{xy} = \tilde{\eta}\left(\frac{\partial u_b}{\partial y} + \frac{\partial v_b}{\partial x}\right), \tag{1b}$$

where $\tau_{ij}$ are the deviatoric stress components. The effective viscosity $\eta$ is a function of the stress invariant:

$$\eta = \tfrac{1}{2}\overline{A}^{-1}\left[\tau_{xz}^2 + \tau_{yz}^2 + \tau_{xy}^2 + \tau_{xx}^2 + \tau_{xx}\tau_{yy} + \tau_{yy}^2\right]^{(1-n)/2}, \tag{2}$$

(the usual Glen's law parameters $A$ and $n$ are treated as constant here, so $\overline{A}$ is taken as a representative average value), and the approximate viscosity, $\tilde{\eta}$, is formed by using the approximations

$$\tilde{\tau}_{xz} = -\rho_i g(s-z)\frac{\partial s}{\partial x} \quad \text{and} \quad \tilde{\tau}_{yz} = -\rho_i g(s-z)\frac{\partial s}{\partial y} \tag{3}$$

for the vertical shear stresses in the stress invariant (see (5) below); thus $\tilde{\eta}$ is given implicitly in terms of $u_b$ and $v_b$ by (1b) and

$$\tilde{\eta} = \tfrac{1}{2}\overline{A}^{-1}\left[\tilde{\tau}_{xz}^2 + \tilde{\tau}_{yz}^2 + \tau_{xy}^2 + \tau_{xx}^2 + \tau_{xx}\tau_{yy} + \tau_{yy}^2\right]^{(1-n)/2}. \tag{4}$$

The vertical compressive stress is taken to be cryostatic, $p - \tau_{zz} = \rho_i g(s-z)$, which allows horizontal force balance to be expressed as

$$\tau_{xz} = -\rho_i g(s-z)\frac{\partial s}{\partial x} + \frac{\partial}{\partial x}\left[\int_z^s \left(2\tau_{xx} + \tau_{yy}\right)\,\mathrm{d}z\right] + \frac{\partial}{\partial y}\left[\int_z^s \tau_{xy}\,\mathrm{d}z\right], \tag{5a}$$

$$\tau_{yz} = -\rho_i g(s-z)\frac{\partial s}{\partial y} + \frac{\partial}{\partial y}\left[\int_z^s \left(\tau_{xx} + 2\tau_{yy}\right)\,\mathrm{d}z\right] + \frac{\partial}{\partial x}\left[\int_z^s \tau_{xy}\,\mathrm{d}z\right], \tag{5b}$$

zero shear stress being applied at the ice surface $z = s(x, y)$. Evaluating (5) at the bed $z = b(x, y)$, and using the sliding law $\boldsymbol{\tau}_b = f(U_b, N_+)\mathbf{u}_b/U_b$, gives

$$\frac{f(U_b, N_+)}{U_b}u_b = -\rho_i g H\frac{\partial s}{\partial x} + \frac{\partial}{\partial x}\left[H\left(2\overline{\tau}_{xx} + \overline{\tau}_{yy}\right)\right] + \frac{\partial}{\partial y}\left[H\overline{\tau}_{xy}\right], \tag{6a}$$

$$\frac{f(U_b, N_+)}{U_b}v_b = -\rho_i g H\frac{\partial s}{\partial y} + \frac{\partial}{\partial y}\left[H\left(\overline{\tau}_{xx} + 2\overline{\tau}_{yy}\right)\right] + \frac{\partial}{\partial x}\left[H\overline{\tau}_{xy}\right], \tag{6b}$$

where $U_b = (u_b^2 + v_b^2)^{1/2}$ is the sliding speed, $H(x, y) = s - b$ is the ice depth, and $\overline{(\cdot)} \equiv \frac{1}{H}\int_b^s (\cdot)\,\mathrm{d}z$ denotes a vertical average.

Equations (6), together with (1b) and (4), constitute a nonlinear system to determine $u_b$ and $v_b$ for a given $N$. From these, (5) then determine the vertical shear stresses $\tau_{xz}$ and $\tau_{yz}$, and the depth dependence of the velocities then follow from (1a), together with (2).

This model is the same as that used by Perego et al. (2012) and suggested by Schoof and Hindmarsh (2010). It is different from the 'L1L2' model of Hindmarsh (2004), which approximates the in-plane strain rates using the surface velocity $\mathbf{u}_s = (u_s, v_s)$ rather than basal velocity. That variant has some advantages (see below), but its solution is slightly more involved because (6) then contains both basal and surface velocities.

### *1.2. Numerical procedure*

The ice flow equations are discretized using finite differences on a rectangular grid (figure 1). Equations (6) and (1b) are solved for a given $N$ by using a Picard iteration to update the approximate viscosity and sliding speed, leaving a linear system to be solved at each iterate for $u_b$ and $v_b$. After convergence to within a specified tolerance, equations (5) determine the vertical shear stresses $\tau_{xz}$ and $\tau_{yz}$, and (1a), together with (2), are integrated to obtain $u$ and $v$. The algorithm has been tested against the ISMIP-HOM benchmark experiments, and compares favourably with other 'higher order' models for the relevant experiments C and D (Pattyn et al., 2008).

The hydrology equations are discretized on the same rectangular grid, writing (M7) in its conservative finite volume form, with channel elements connecting the nodes on which the pressure and sheet depth are defined (figure 1). For fixed basal shear stress and sliding velocity, equations (M3)-(M7) together

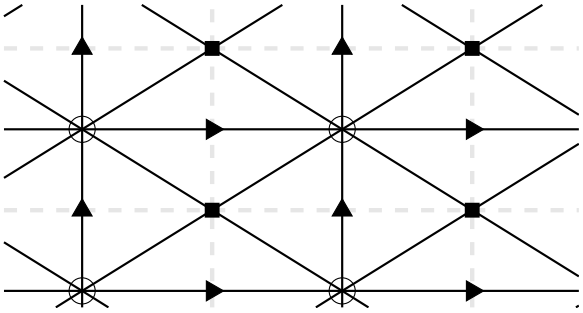

Figure 1: Grid used for numerical computations. Circles are the nodes, on which $p_w$ and $h$ are defined; dashed lines show the edges of the finite volumes with the components of $\mathbf{q}$ defined on the triangles. Channels connect the nodes along the solid lines ($\mathbf{x}_c$) and are defined at their centres on the triangles and squares. Moulins are defined on a selection of the nodes ($\mathbf{x}_m$). Ice velocity components $u_b$ and $v_b$ are defined on the edges (triangles), normal stresses $\tau_{xx}$ and $\tau_{yy}$ are defined on the nodes (circles), and in-plane shear stresses $\tau_{xy}$ are defined on the corners (squares). Sliding speed and effective pressure are calculated on the nodes. A vertical extrusion of this grid, normalized by the local ice thickness, is used to calculate the viscosity on the nodes and the surface velocity on the edges. Most of the calculations have 100-by-100 nodes, with 16 vertical layers.

constitute a non-linear system for the evolution of $p_w$, $h$ and $S$, which is solved implicitly at each timestep using a Newton method (the final dissipation term in $(M6)_2$ is included explicitly, for reasons of speed).

Each such timestep of the hydrology equations is followed by an updated solution for the ice flow using the new values of effective pressure, so the algorithm successively alternates between the two model components. A variable timestep is used, based upon the success of previous iterations. Generally timesteps on the order of hours are required during rapid evolution of the drainage system; much longer timesteps can be taken during winter.

A number of regularizations are applied to expedite the computations. In the friction law in (6), $U_b$ in the denominator is replaced with $(U_b^2 + U_\varepsilon^2)^{1/2}$, $U_\varepsilon = 1$ cm y$^{-1}$ being a small regularizing velocity. A small additional strain rate $\dot{\varepsilon}_\varepsilon = 10^{-13}$ s$^{-1}$ is added to the longitudinal strain rates in the viscosity (4). The non linear part of the potential gradient in $(M3)_2$, $\Psi = |\partial\phi/\partial x|$, is replaced by $(\Psi^2 + \Psi_\varepsilon^2)^{1/2}$ where $\Psi_\varepsilon = 1$ kg m$^{-2}$ s$^{-2}$. Finally, a small regularizing pressure $p_\varepsilon = 10^3$ Pa is added to $p_i$ in the denominator of (M5b).

### *1.3. Comments on the ice flow model*

The ice flow model is an approximation to the full Stokes equations that is strictly valid for small aspect ratios and rapid sliding. Like many asymptotic models it may perform adequately outside of these conditions, but care is required. In this study, with its simple geometry and boundary conditions, the issue of potential concern is the basal shear stress: the model is not designed to deal with variations on a scale smaller than the ice thickness, but the effective pressure varies on smaller scales. I do not believe this is a reason to discredit these results, but it should signal some caution.

The effect of the membrane stresses in (6) is to smooth the solution for $\mathbf{u}_b$, so a locally high spike in effective pressure (say) does not cause an abrupt low spike in $\mathbf{u}_b$, as would be predicted by the shallow ice approximation. In this sense, the effect of small scale pressure variations is naturally smoothed out by the model. On the other hand, that smoothing of $\mathbf{u}_b$ is at the expense of creating a spike in shear stress $\tau_{xz}$ (5) in order to balance the high basal shear stress due to the spike in effective pressure. That enhanced shear stress leads to greater internal deformation, and (perversely) a local increase in the predicted surface velocity. Close inspection of figure M2 reveals this slightly elevated surface velocity above the location of the low-pressure subglacial channels; I believe this is an artifact of the model and one should not read anything into these small scale velocity differences. For this reason, I chose to deliberately suppress internal deformation (by choosing a higher value for $\overline{A}$) and ensure that the majority of surface motion is due to basal sliding (around 80% during winter).

This issue is also evident when testing against the ISMIP-HOM experiments: when the smallest scale variations in $\beta^2$ are imposed in the friction law $\boldsymbol{\tau}_b = \beta^2 \mathbf{u}_b$, a local increase in surface velocity is predicted where $\beta^2$ is largest, resulting from the artificially enhanced internal deformation. A similar feature appears in the work of Perego et al. (2012).

Significant short length scale variations in effective pressure likely result in non-hydrostatic vertical compressive stress, requiring the full Stokes equations to properly resolve. A slight improvement might be gained by using the three-dimensional 'Blatter-Pattyn' approximation (Pattyn, 2003), or even the 'L1L2' cousin of the current model, in which the membrane stresses act to smooth surface velocities rather than basal velocities. Experiments using that variant suggest that the same issue is avoided in that case; indeed one might conjecture that it is more appropriate to use surface strain rates when approximating the longitudinal stresses since the majority of those stresses are transferred near the top of the ice column (where the viscosity is highest). Another avenue to explore might be to take a local average of the effective pressure in the friction law.


Hindmarsh, R. C. A., 2004. A numerical comparison of approximation to the Stokes equations used in ice sheet and glacier modeling. J. Geophys. Res. 109.

Pattyn, F., 2003. A new three-dimensional higher-order thermomechanical ice sheet model: Basic sensitivity, ice stream development, and ice flow across subglacial lakes. J. Geophys. Res. 108.

Pattyn, F., Perichon, L., Aschwanden, A., Breuer, B., de Smedt, B., Gagliardini, O., Gudmundsson, G. H., Hindmarsh, R., Hubbard, A., Johnson, J. V., Kleiner, T., Konovalov, Y., Martin, C., Payne, A. J., Pollard, D., Price, S., Rückamp, M., Saito, F., Souček, O., Sugiyama, S., Zwinger, T., Feb. 2008. Benchmark experiments for higher-order and full Stokes ice sheet models (ISMIP-HOM). The Cryosphere Discussions 2, 111–151.

Perego, M., Gunzburger, M., Burkardt, J., 2012. Parallel finite-element implementation for higher-order ice sheet models. J. Glaciol. 58, 76–88.

Schoof, C., Hindmarsh, R. C. A., 2010. Thin-film flows with wall slip: an asymptotic analysis of higher order glacier flow models. Q. J. Mechanics. Appl. Math. 63, 73–114.